MICROSTRUCTURE ARCHITECTURE DEVELOPMENT IN METALS AND ALLOYS BY ADDITIVE MANUFACTURING USING ELECTRON BEAM MELTING

L. E. Murr,[1,2] S. M. Gaytan,[1,2] D. A. Ramirez,[1,2] E. Martinez,[1,2] J. L. Martinez,[1,2] D. H. Hernandez,[1,2] B. I. Machado,[1] F. Medina[2] and R. B. Wicker[2]
[1]Department of Metallurgical and Materials Engineering
The University of Texas at El Paso, El Paso, TX 79968 USA
[2]W. M. Keck Center for 3D Innovation
The University of Texas at El Paso, El Paso, TX 79968 USA

Reviewed, accepted September 23, 2010

Abstract

The concept of materials with controlled microstructural architecture (MCMA) to develop and fabricate structural materials with novel and possibly superior properties and performance characteristics is a new paradigm or paradigm extension for materials science and engineering. In the conventional materials science and engineering paradigm, structure (microstructure), properties, processing, and performance features are linked in the development of desirable materials properties and performance through processing methodologies which manipulate microstructures. For many metal or alloy systems, thermomechanical treatment combining controlled amounts of plastic deformation with heat treatment or aging cycles can achieve improved mechanical properties beyond those attainable by conventional processing alone (such as rolling or forging for example) through controlled microstructure development. In this paper we illustrate a new concept involving the fabrication of microstructural architectures by the process development and selective manipulation of these microstructures ideally defining material design space. This allows for the additional or independent manipulation of material properties by additive manufacturing (AM) using electron beam melting (EBM). Specifically we demonstrate the novel development of a carbide ($M_{23}C_6$) architecture in the AM of a Co-base alloy and an oxide (Cu_2O) precipitate-dislocation architecture in the AM of an oxygen-containing Cu. While more conventional processing can produce various precipitate microstructures in these materials, EBM produces spatial arrays of precipitate columns or columnar-like features often oriented in the build direction. These microstructural architectures are observed by optical microscopy and scanning and transmission electron microscopy. Prospects for EBM architecture development in precipitation-hardenable Al alloys is also discussed. In the EBM build process using precursor powders, the electron beam parameters (including beam focus, scan speed and sequencing) produce localized, requisite thermodynamic regimes which create or organize the precipitate-related spatial arrays. This feature demonstrates the utility of AM not only in the fabrication of complex components, but also prospects for selective property design using CAD for MCMA development: a new or extended processing-microstructure-property-performance paradigm for materials science and engineering in advanced manufacturing involving solid free-form fabrication (SFF).

Introduction

We have recently observed unique spatial arrays of $Cr_{23}C_6$ precipitate column architectures in Co-base alloy components fabricated by EBM (Gaytan, *et al*., 2010 a,b) Almost simultaneously, we have observed similar architectural features in an oxygen-containing Cu where Cu_2O precipitates and associated dislocation cell-like arrays occurred in EBM fabricated Cu components (Ramirez, *et al.*, 2010). These observations suggest prospects for utilizing AM and EBM as a unique processing route capable of producing controlled microstructural architectures.

In this paper we examine these microstructural architectures in EBM fabricated components using a Co-base alloy (Co-26Cr-6Mo-0.2C) and a Cu (99.8% ~0.2% oxygen) precursor powder; both having the fcc crystal structure with a=3.6Å and the space group: O^5_H-FM^3M.

Methods and Procedures

While we have reviewed the EBM-AM system in some detail elsewhere (Gaytan *et al*., 2010; Ramirez *et al.*, 2010; Murr *et al.*, 2009; Gaytan *et al.*, 2009), it will provide a useful context if we briefly describe the EBM system, especially because it is the process features which create the unique microstructural architectures to be illustrated. Figure 1 illustrates the ARCAM (A2) EBM system and fundamentals of the AM process which begins with precursor powders shown. Figure 1A shows a cutaway schematic illustrating the electron gun at (1) which operates nominally at 60kV, and the electromagnetic lens system in the electron optical column (2), which includes the beam scan coils which raster the beam to preheat and melt specific layer areas as directed by the CAD program. Powders, as illustrated in SEM images in Figure 1 B-D, are loaded into hoppers (3) which gravity feed the powder onto the build table where it is raked (4) into layers ranging from ~50 to 100 µm depending upon the powder particle size and size distribution which is apparent on examining, comparatively, Figure 1 B-D. The build itself shown at (5) in Figure 1 begins on a heated base plate: steel in the case of the Co-base alloy (Figure 1B), and copper in the case of the Cu AM (Figure 1C).

As each layer is raked (Figure 1A) the electron beam (with some optimum focus depending upon powder layer thickness, melting point, etc.) is rastered in ~11 passes to preheat the layer, followed by a melt scan. These scans are rastered in the x and the y-directions across the raked layer. Preheat scan speeds range from $1\text{-}1.5\text{x}10^4$ mm/s while melt scans range from ~50-400 mm/s (Gaytan *et al.*, 2010a, 2010b); Ramirez *et al.*, 2010). The corresponding beam currents also vary from ~30 mA for preheat scan passes to ~5 mA for the slower melt scans.

In this paper, we explore and compare Co-base alloy (Co-26Cr-6Mo-0.2C) builds and 99.8% Cu builds (Figure 1 B and C). The Al-6061 powder in Figure 1D illustrates the availability of suitable Al-alloy powder, but we will only discuss EBM build concepts based on this alloy, and in the context of microstructural architectures observed in Co-base alloy and Cu component fabrication.

EBM fabricated Co-base alloy components consisted of cylinders measuring 1 cm x 8 cm and rectangular blocks measuring 1 cm x 5 cm x 6 cm. Sections and coupons were extracted from these components in various sizes and embedded in standard, metallographic expoxy mounts, ground, polished, and etched with a 6:1 HCl : H_2O_2 (3%) solution. (Gaytan *et al.* (2010a)). Cu components consisting of smaller cylinders were similarly mounted, polished, and etched with solution. (Ramirez *et al.*, 2010). Optical metallography for polished and etched

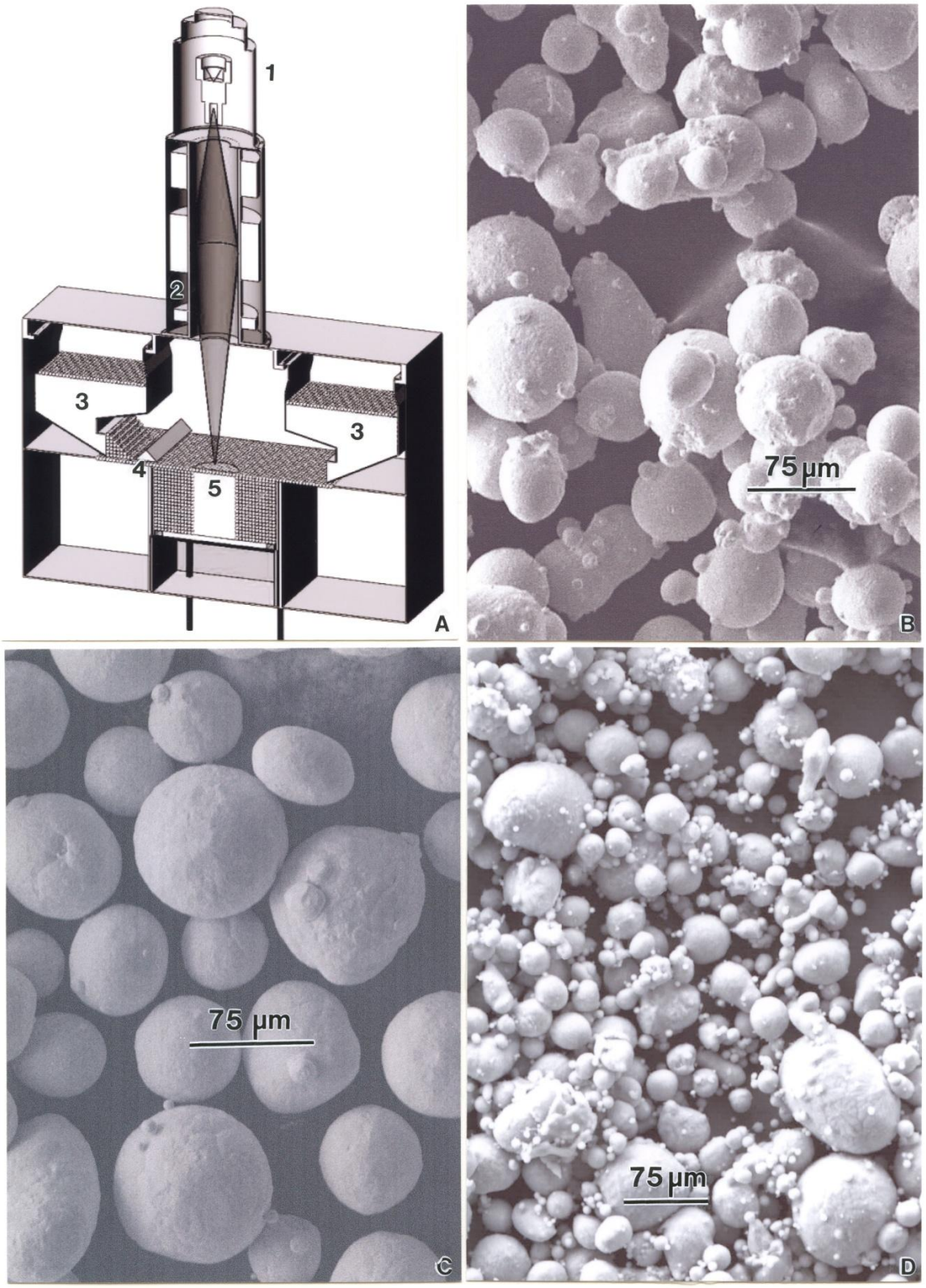

Figure 1. EBM system and examples of precursor powders. (A) Arcam A2 EBM system schematic. (B) Co-26Cr-6Mo-0.2C powder. (C) Cu powder. (D) Al-6061 powder.

specimens was performed using a Reichart MEF4 A/M metallograph. Specimens were also examined in a Hitachi S4800 field emission scanning electron microscope operated at 20kV.

Coupons extracted from fabricated Co-base alloy and Cu components were also sliced to thin sections ~0.2 mm thick, mechanically dimpled, punched into 3 mm discs, and electropolished in a Struers Tenupol 5, dual-jet electropolisher. A solution of 15% perchloric acid and 85% acetic acid was used for the Co-base alloy while a solution of 825 mL H_2O, 375 mL ethanol, 300 mL phosphoric acid, 75 mL propanol and 2.5 g urea was used to electropolish electron transparent regimes in the Cu sections. These electropolished, 3 mm discs were examined in a Hitachi H9500 transmission electron microscope at 300kV accelerating potential, employing a goniometer-tilt stage and a digital CCD imaging camera.

Results and Discussion

Co-Base Alloy Microstructural Architectures

There are a number of metal – carbon precipitates which can form in Co-base alloys under varying thermomechanical processing conditions including M_7C_3, $M_{23}C_6$ and M_6C (M is usually or dominated by Cr). These carbide precipitates are often distributed homogeneously within the grain structures and/or preferentially precipitated within the grain boundaries (Crook, 1993).

Figure 2 illustrates a representative view of $M_{23}C_6$ precipitates formed in EBM fabricated Co-base alloy cylinders in this study (Gaytan *et al.*, 2010a). The horizontal plane perpendicular to the build direction (Figure 1A) shows a regular (orthogonal) spatial array characteristic of carbide precipitate columns, or a columnar architecture extending parallel to the build direction (arrow in Figure 2). This microstructural architecture is unique to any contemporary materials processing and specific to AM using EBM.

Figure 3 illustrates a magnified view of these precipitate architectures observed in the TEM. The characteristic cubic (a= 10.6 Å; space group: FM3M) crystal structure for the $M_{23}C_6$ precipitates is readily apparent from the precipitate morphologies, having sizes ranging from ~50 to 200 nm. These precipitates are non coherent with the fcc Co matrix a = 3.6 Å. The spatial arrays of columnar carbides in Figures 2 and 3 are spaced 1 to 3 µm while the carbide spacing along the columns averages ~<0.1 µm.

Figure 4 shows a schematic view for the EBM processing features creating these precipitate architectures as a consequence of the spatial regimes created by x-y layer scanning of the electron beam creating $M_{23}C_6$ precipitate columns as the build is extended layer-by-layer.

In addition to $M_{23}C_6$ precipitate arrays, this microstructure is intermixed with stacking faults or twin-faults which are also prominent in conventional Co-base alloy processing (Atamert and Bhadeshia, 1989). Figure 5 illustrates these microstructural features as observed by TEM in the horizontal plane of a build (normal to the build direction) as illustrated in Figure 2. These stacking-fault arrays are relatively dense, but irregularly dispersed throughout the $M_{23}C_6$ precipitate architecture as shown typically in the overview in the horizontal build plane shown in Figure 6 which also shows grain and sub-boundaries.

When the EBM Co-base alloy products are annealed (ASTM F75 standard: 1200-1430°C (~8 h), the $M_{23}C_6$ precipitate architectures are solutionized, leaving only selective grain boundary carbides (illustrated by electron diffraction and XRD: Gaytan et al., 2010a) and a reduced density of stacking faults in the resulting equiaxed grain structure. These features are illustrated in Figures 7 and 8 which provide a rather dramatic contrast in comparison with Figures 5 and 6

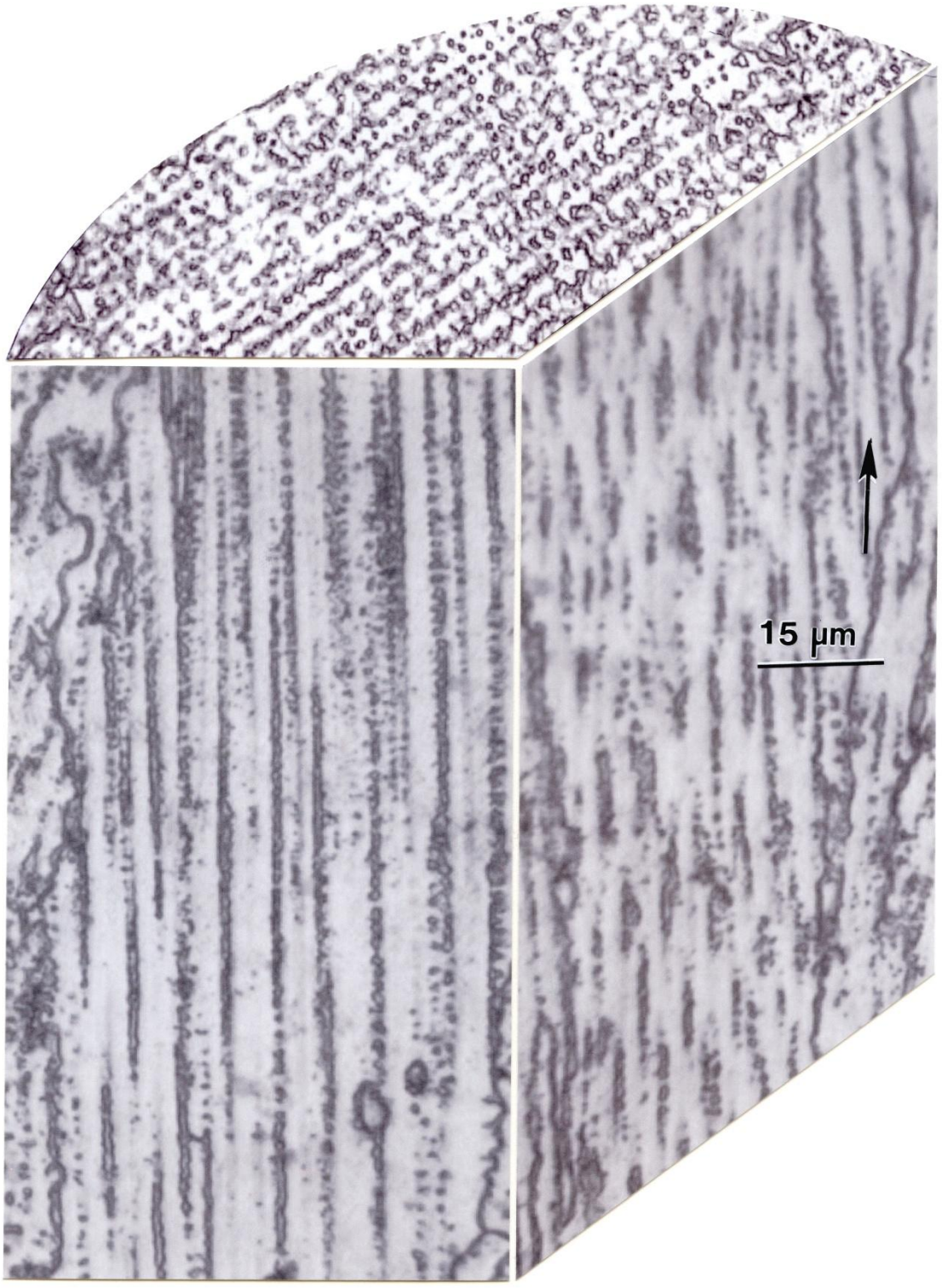

Figure 2. Optical microscope 3D image composition representing microstructural architecture in EBM fabricated Co-26Cr-6Mo-0.2C component. Arrow indicates build direction.

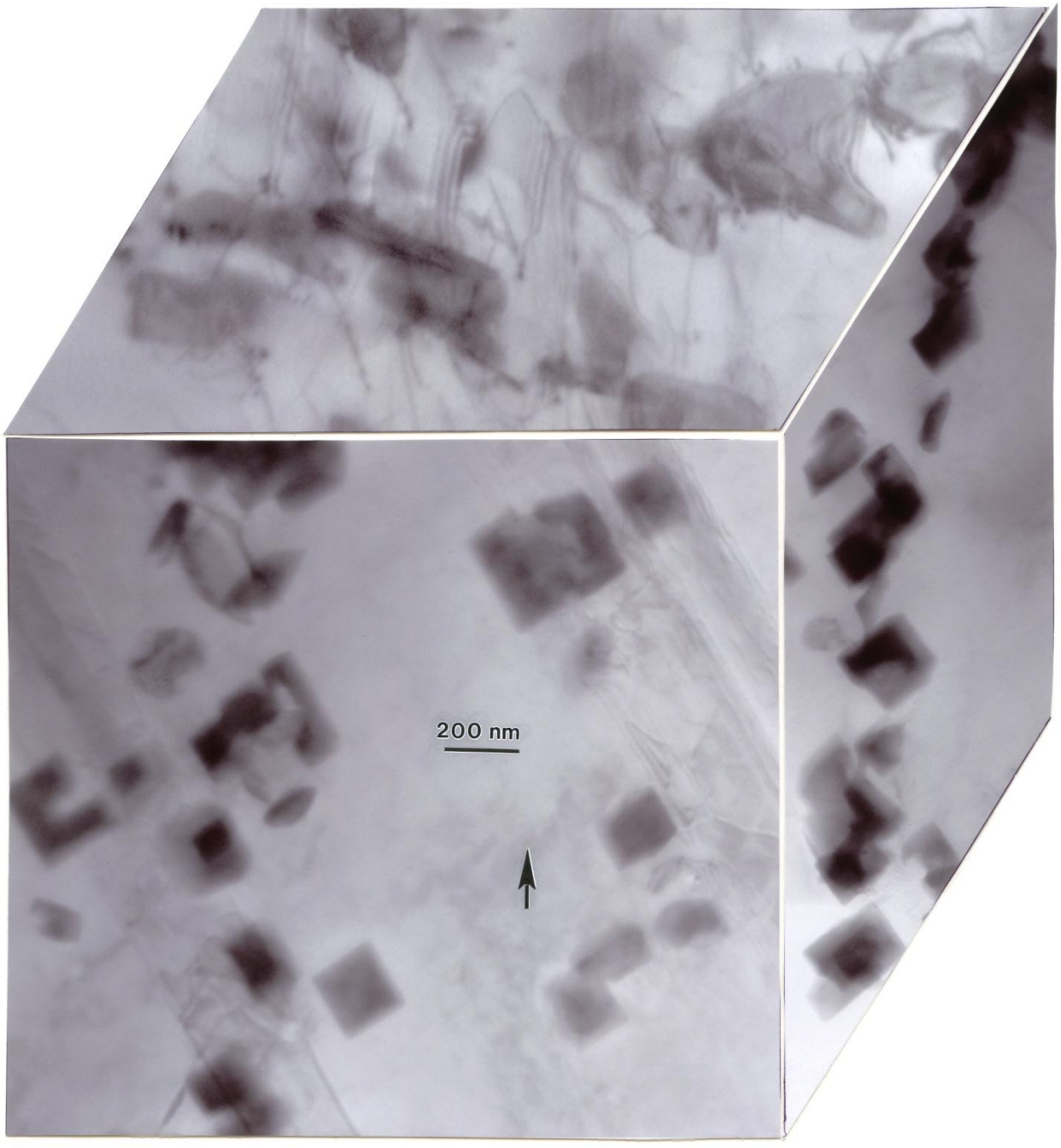

Figure 3. TEM bright-field image of 3D segment for architecture shown in Figure 2. Note stacking-fault images in surface and vertical planes intermixed with $Cr_{23}C_6$ precipitate columns. The cube (001) edges of the carbides are parallel to the trace of the stacking faults (along <110>).

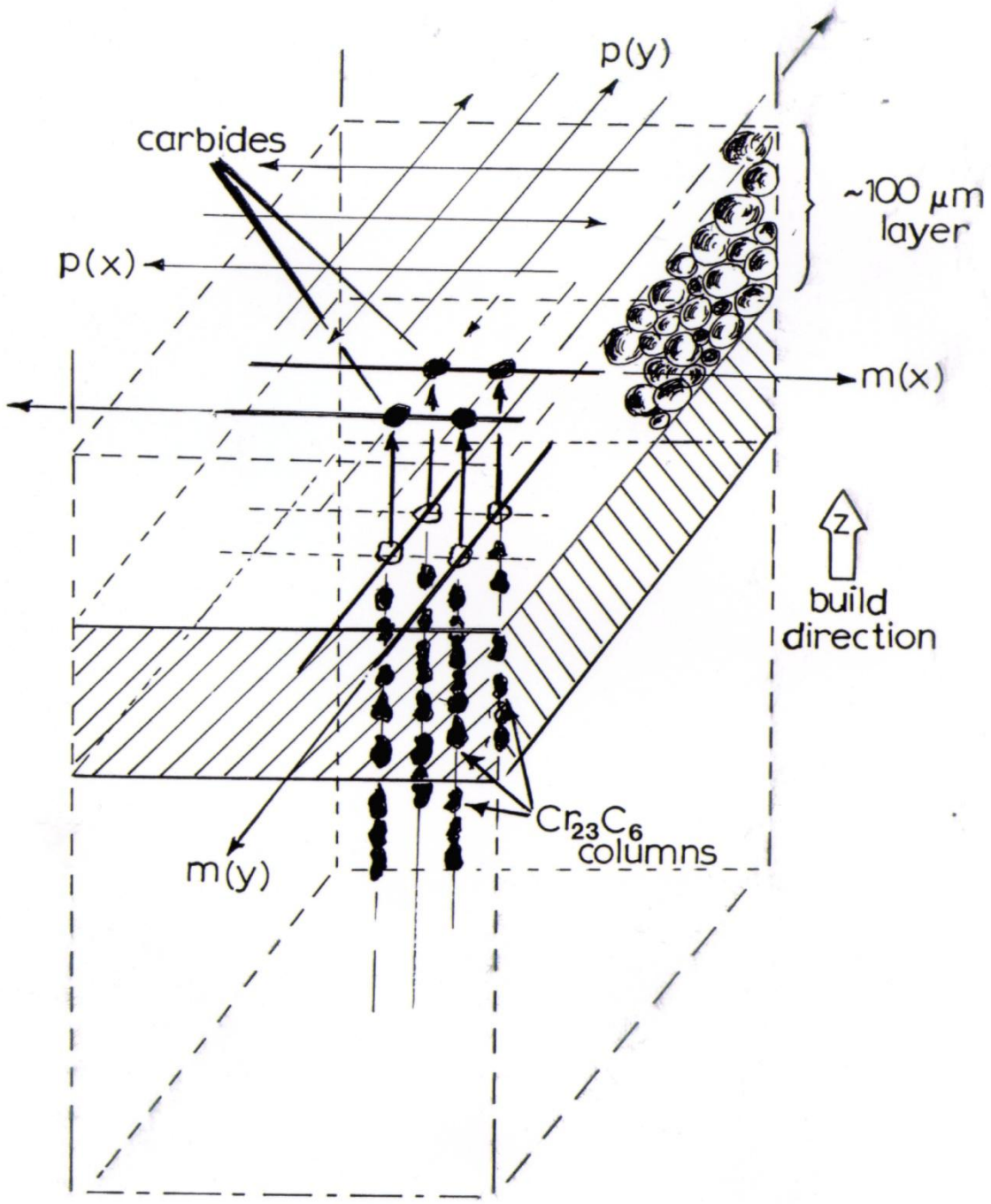

Figure 4. Schematic diagram depicting EBM electron beam scan geometry creating thermally requisite zones for $Cr_{23}C_6$ precipitate formation and columnar growth in build direction (From Gaytan *et al.*, 2010a).

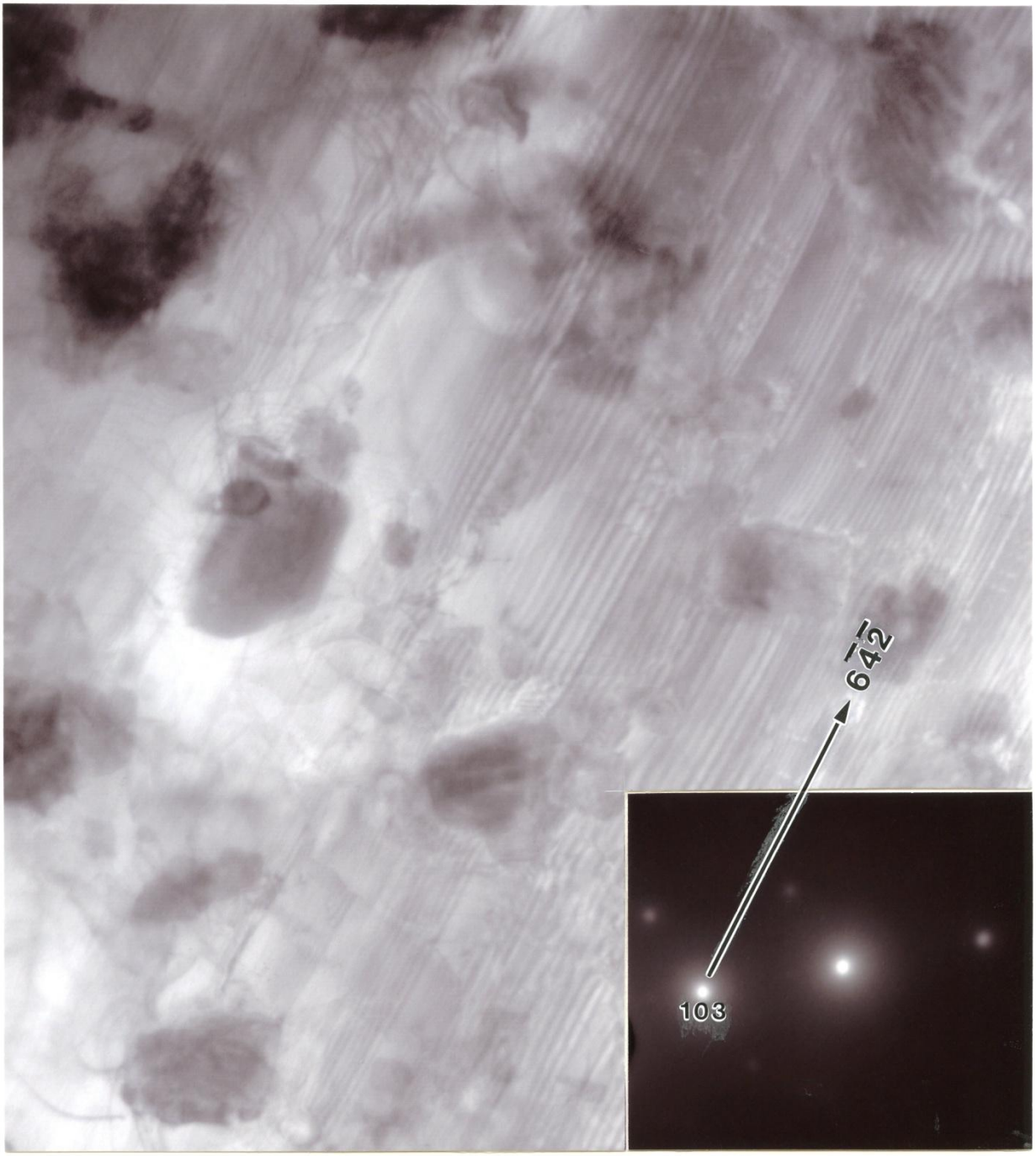

Figure 5. TEM bright-field image showing dense stacking-fault arrays and carbide precipitates in the horizontal plane for an extracted Co-base alloy sample. Surface orientation as noted in selected-area electron diffraction (SAED) pattern is (103). As indicated by the [6] trace direction the fault plane is (111).

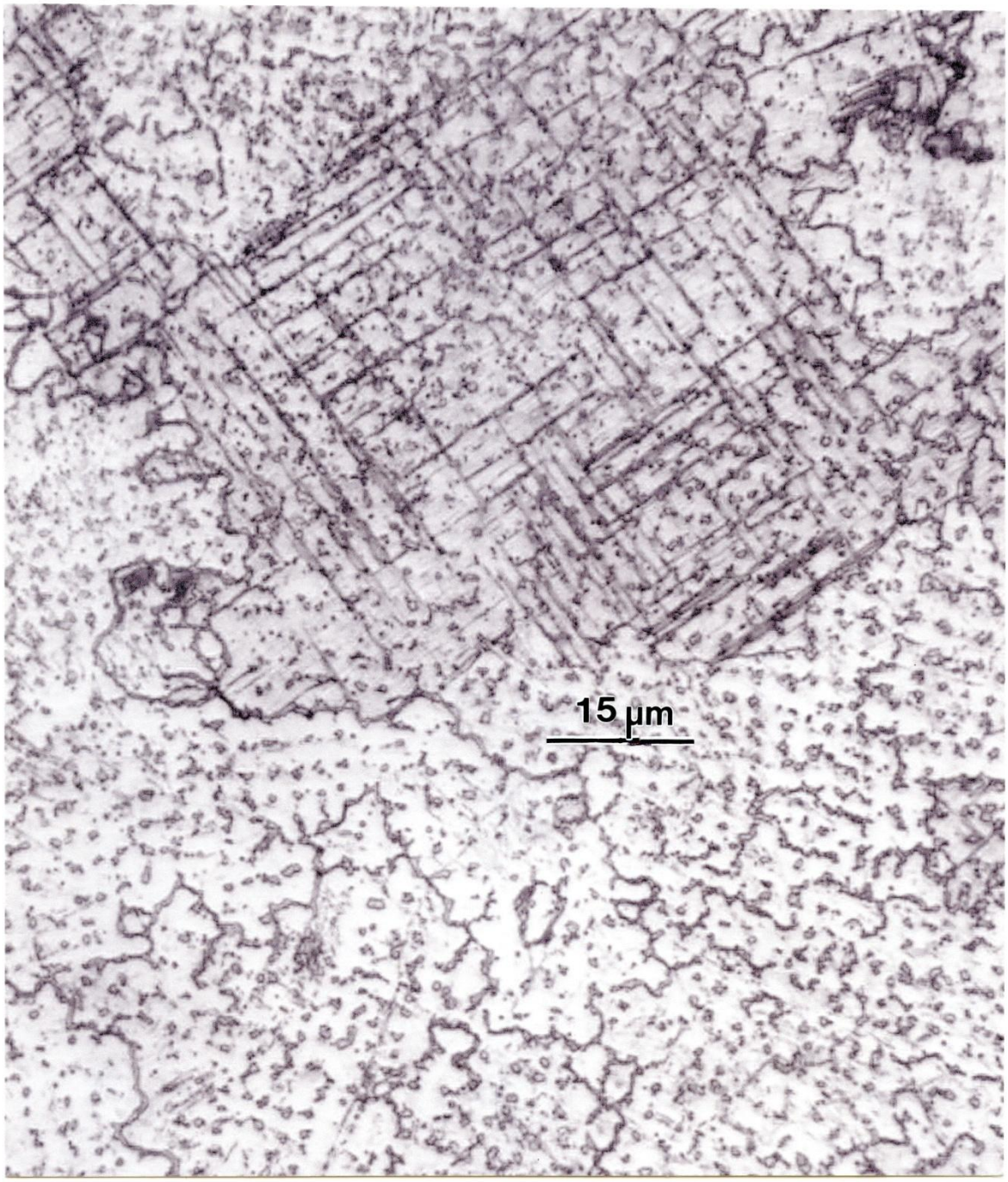

Figure 6. Optical microscope horizontal plane image expansion for a Co-base alloy component illustrating twin-fault features at 90° characteristic for (100) surface orientation. The faulted area is also representative of actual grain dimensions which are difficult to distinguish.

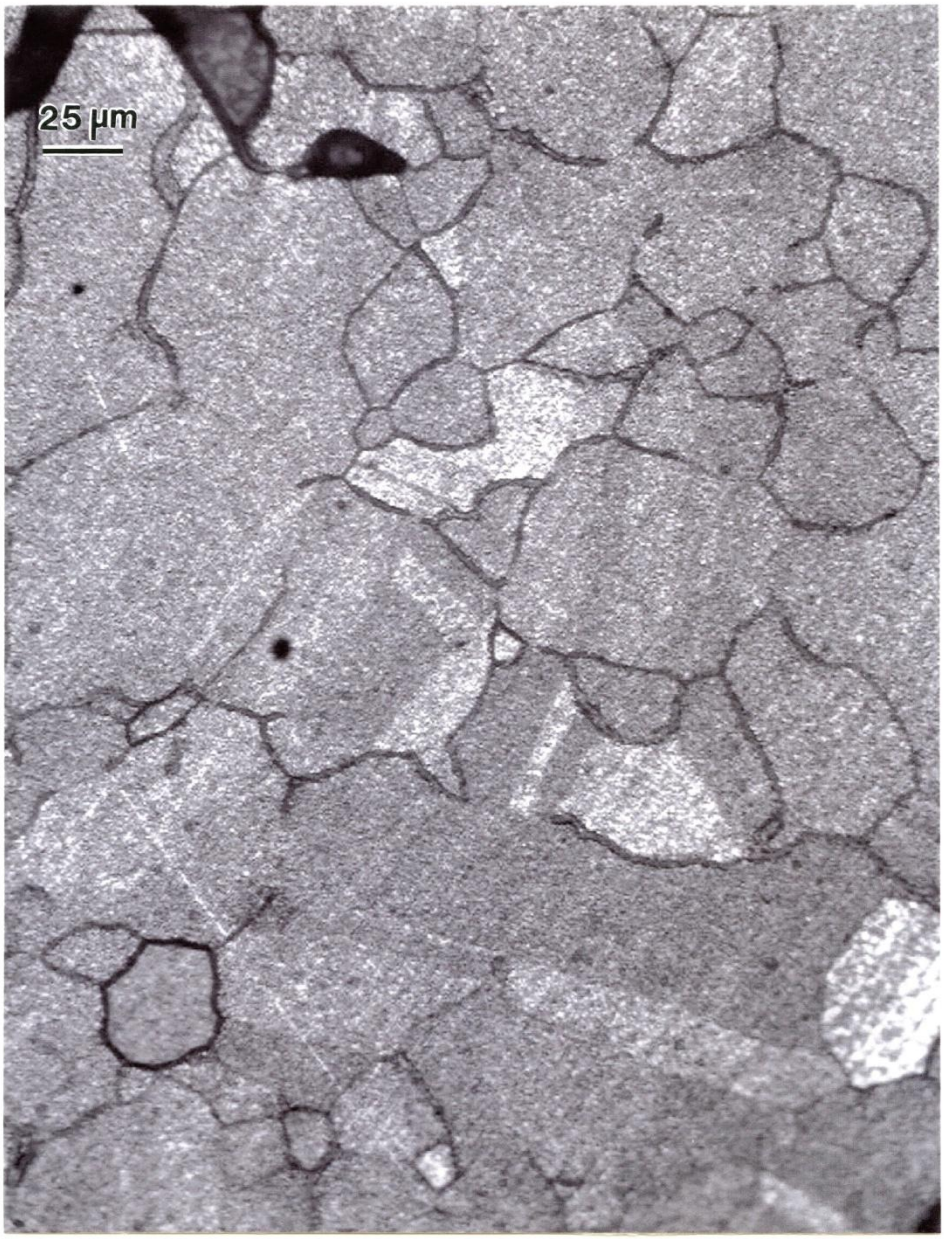

Figure 7. Equiaxed grain (including coherent twin grains) in annealed Co-26Cr-6Mo-0.2C fabricated by EBM. Note $Cr_{23}C_6$ carbides selectively etched in selective grain boundaries.

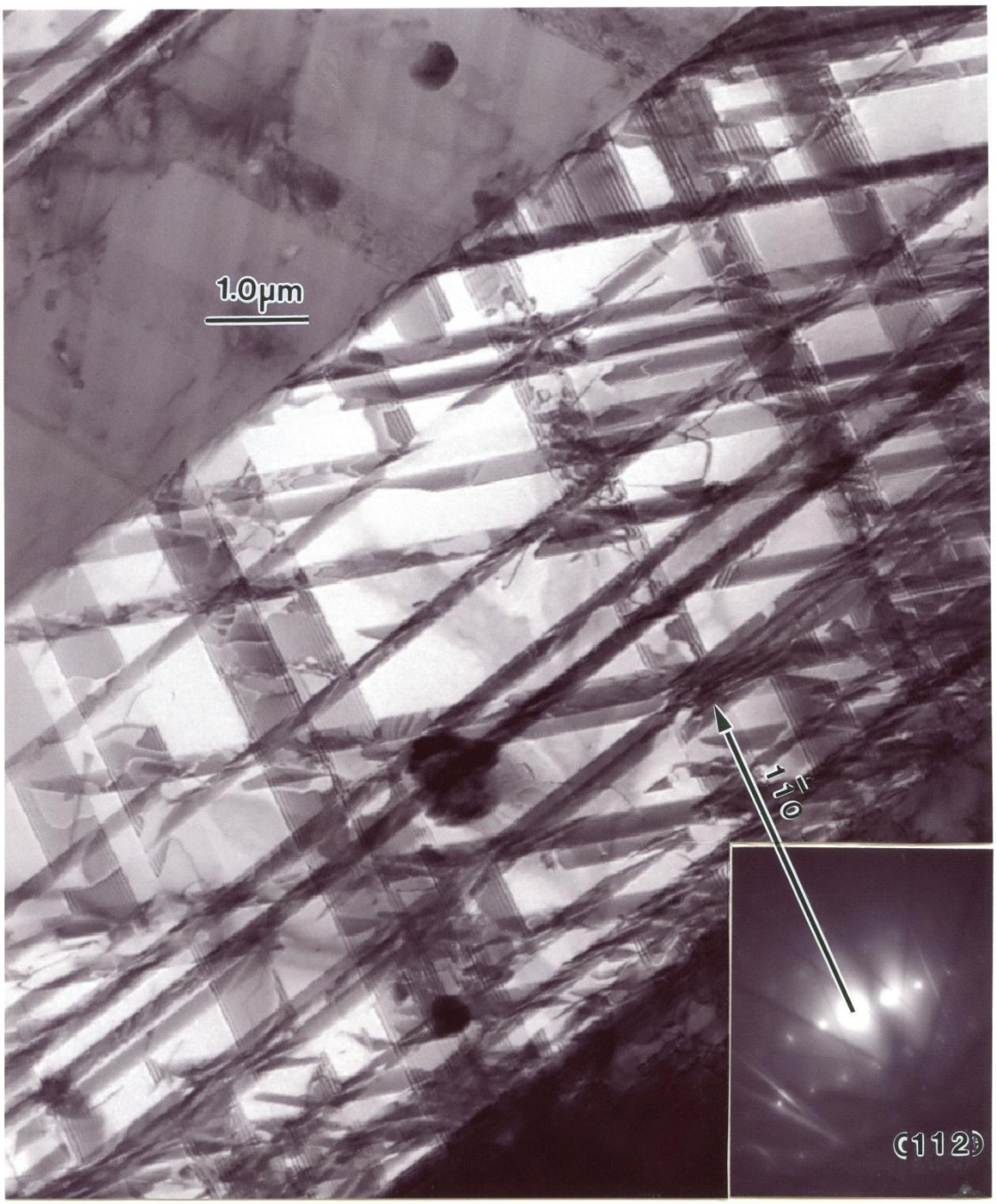

Figure 8. Typical TEM bright-field image showing stacking faults in a twin grain characteristic of Figure 7. Note surface orientation and one fault-variant trace direction in SAED pattern insert.

in retrospect. Notice the stacking faults with an annealing twin grain in Figure 8 and the corresponding annealing twins shown in the annealed grain structure in Figure 7 (light or white grains). The stacking faults account for a significant portion of the hardness.

Cu Microstructural Architecture

In contrast to Figure 2 for the Co-base alloy, Figure 9 shows a corresponding 3D image composition for an EBM fabricated Cu cylinder exhibiting a Cu_2O precipitate architecture which, although similar to the $M_{23}C_6$ precipitate architecture in Figure 2, is considerably more irregular. In contrast to the more regular orthogonal horizontal surface spatial $M_{23}C_6$ precipitate arrays in Figures 2 and 6, those for Cu_2O precipitate arrays in Figure 9 are more irregular, cell-like, because of the reduced melting point and thermal relaxation in the EBM Cu fabrication.

As in the case for $M_{23}C_6$ precipitate observations in the optical metallographic views in Figures 2 and 6, the Cu_2O precipitate arrays in Figure 9 arise by selective etching of the precipitates, forming regular arrays of pits. These features are particularly apparent from the SEM images shown in Figure 10 which shows cubic and rectangular-like pits in the vertical plane (parallel to the build direction) corresponding to the Cu_2O precipitate columns shown near the left edge for the image composition in Figure 9. Like the cubic $M_{23}C_6$ precipitate structures, the Cu_2O (cuprite) precipitates are also cubic (a=4.3 Å; space group: O^4_H PN3M), and aggressively reacted with H_2SO_4. XRD analysis indicates several, prominent Cu_2O peaks: (200), (220), (222).

Figure 11 shows an enlarged view for the horizontal surface perspective for Cu_2O precipitate arrays illustrating the cell-like microstructure while Figure 12 shows these cell-like microstructures to be composed of noncoherent Cu_2O precipitates in a dense cell-like dislocation structure with dislocations emanitating from and corrected with the precipitates. The TEM view in Figure 12 corresponds very closely to the broader optical microscopic view shown in Figure 11. Figure 13 illustrates the precipitate-dislocation arrays at higher magnification. The cuboidal appearance is apparent while selective etching and pitting of precipitates is also apparent, and supporting of the pitting illustrated in Figure 10.

In contrast to the EBM schematic for the $Cr_{23}C_6$ precipitate architecture creation in the EBM fabrication of a Co-base alloy as shown in Figure 4, Figure 14 shows a corresponding, schematic modification for the EBM-produced Cu_2O-dislocation architecture.

The actual grain sizes in the EBM components is often related somewhat to the powder particle size distribution, although very irregular grain structures and grain boundaries are observed as illustrate in the example shown in Figure 6. Figure 15A shows the copper base-plate microstructure characteristic for annealed fcc metals and alloys, and similar to the fcc annealed grain structure for the Co-base alloy shown in Figure 7. In contrast, Figure 15B shows a broader section for a horizontal plane section for a Cu build, which illustrates, in comparison with Figures 9 and 11, the variability of the microstructures and spatial architecture arrays, which are not as consistent as those for the Co-base alloy shown in Figure 2. A more specific comparison might involve describing the horizontal plane in Figure 2 in terms of a regular 2D tessallation, while that in Figure 9 in contrast can be regarded as an irregular 2D tessallation.

Of course it should be noted that Cu_2O precipitates in Cu are largely an anomalie not generally desirable. However, in this case, it has provided an interesting contrast to $Cr_{23}C_6$ precipitates created and organized by the EBM processing of Co-base alloy powder.

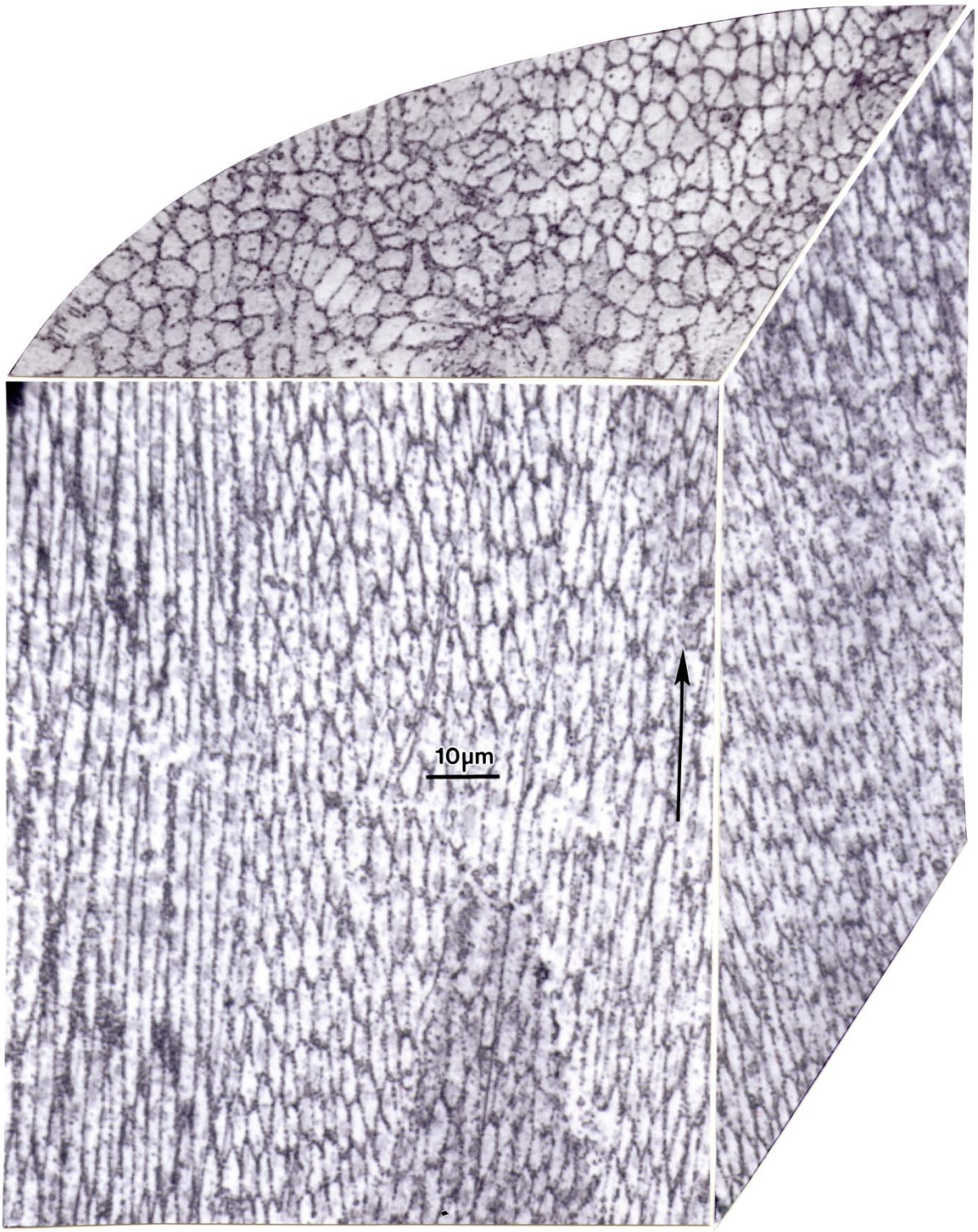

Figure 9. Optical microscope 3D image composition representing microstructural architecture development in EBM fabricated Cu component containing Cu_2O precipitates. Arrow indicates build direction.

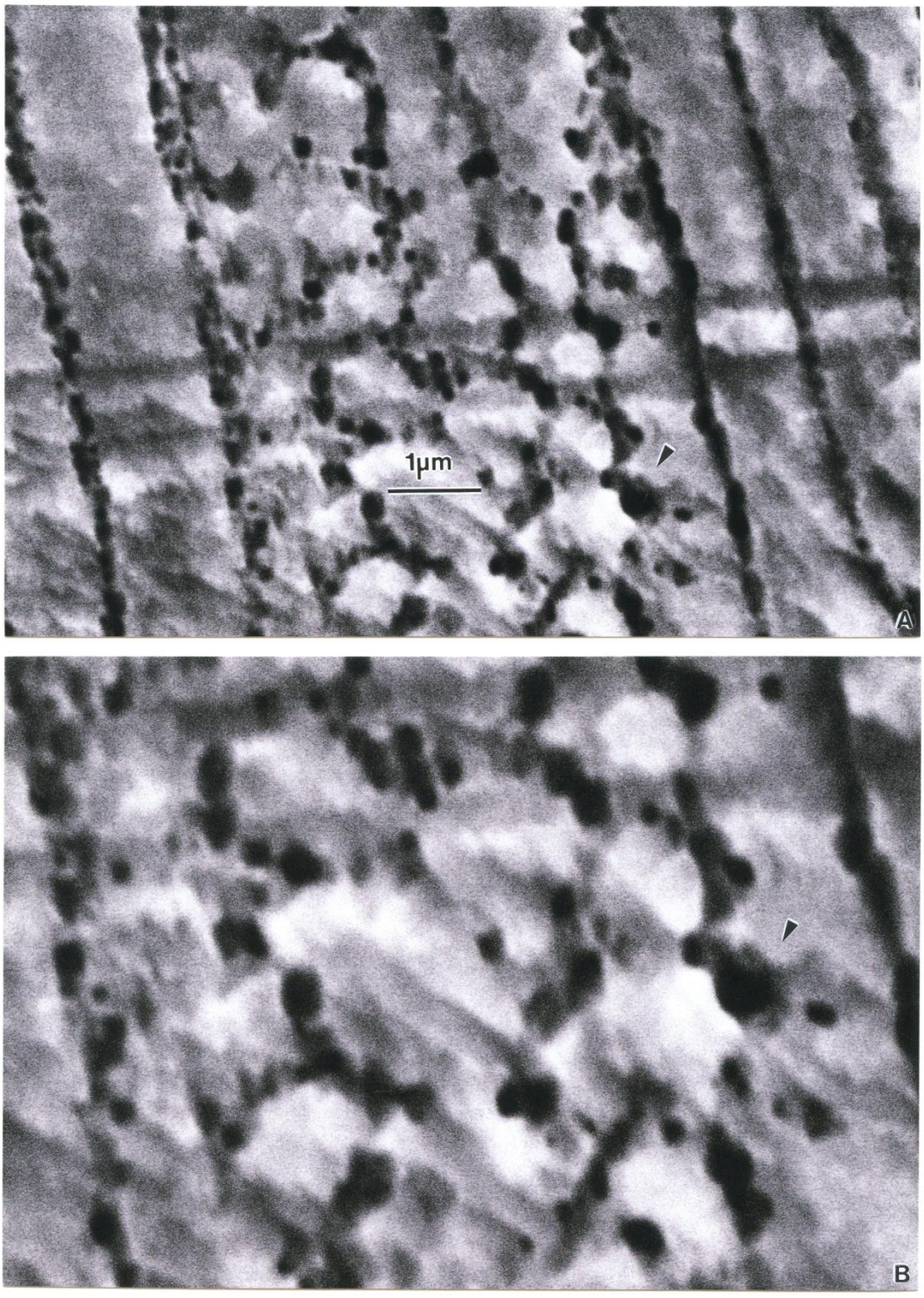

Figure 10. SEM views (A and B) for etch pits characterizing Cu_2O column-like architectures in the vertical plane parallel to the build direction illustrated in Figure 9. (B) shows a magnified view for reference marked by arrow in (A) and (B). Note rectangular and cuboidal etch pits.

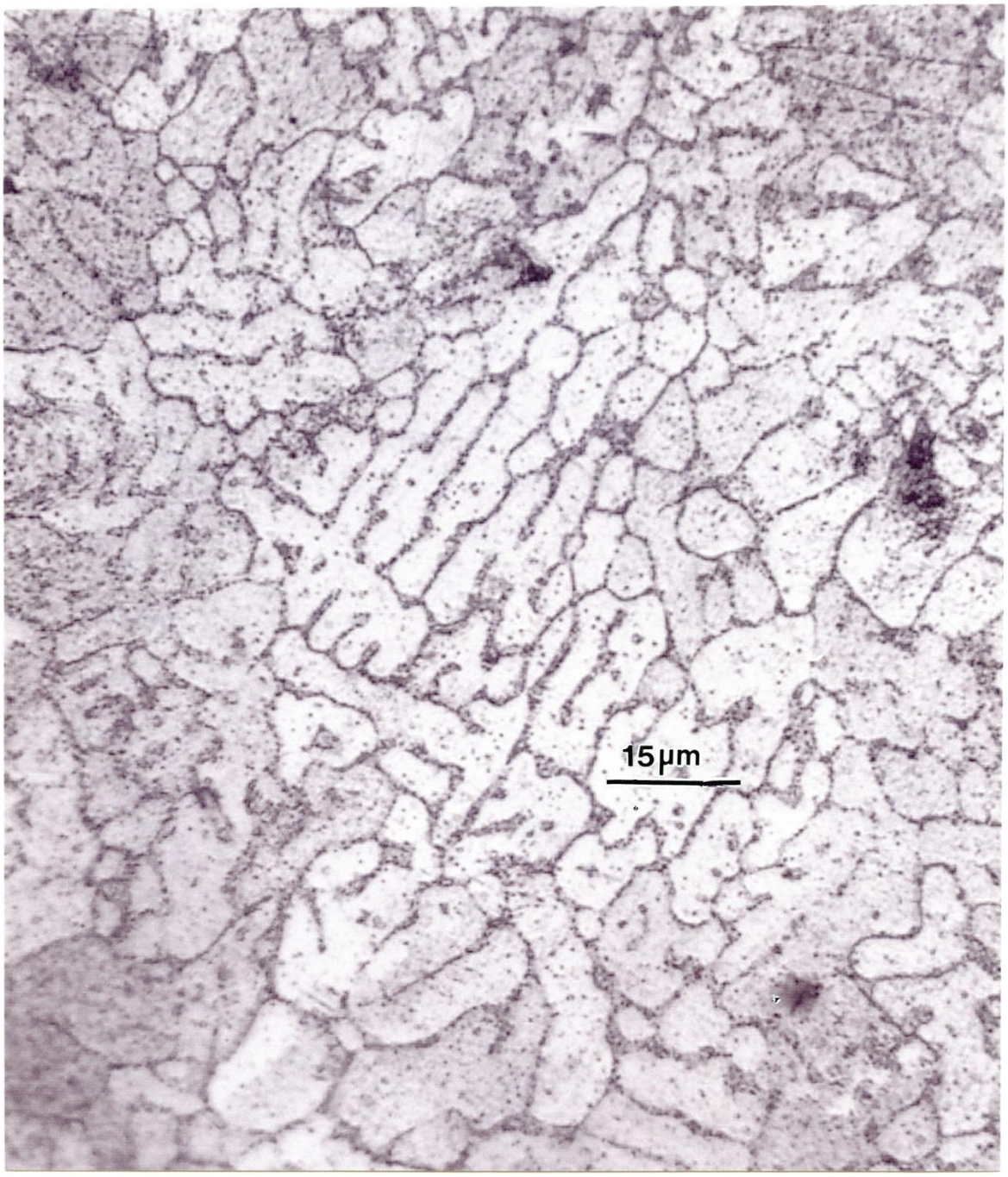

Figure 11. Expanded horizontal surface view (normal to the EBM build direction) for EBM fabricated Cu specimen showing irregular cell-like arrays by selective etching.

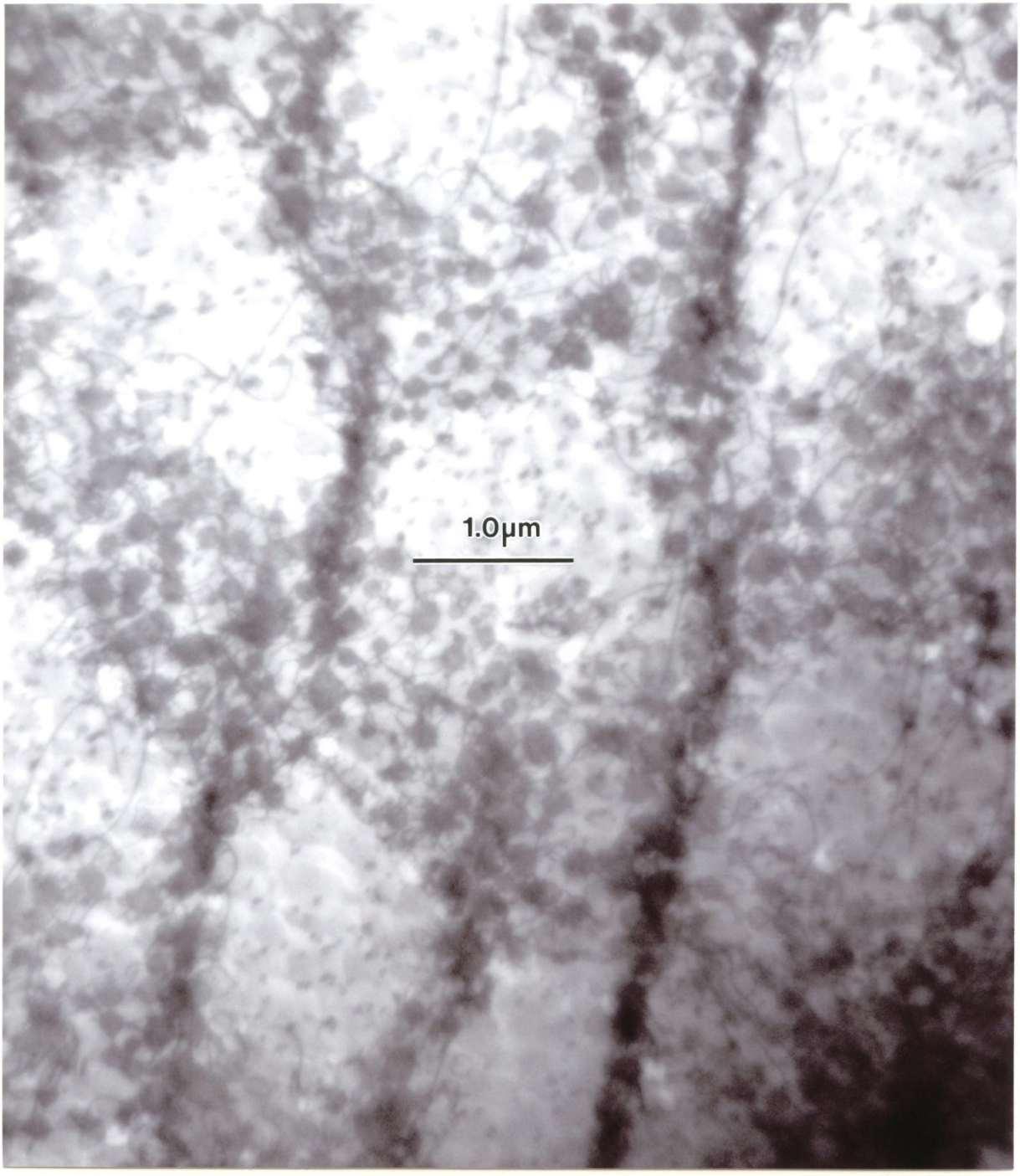

Figure 12. TEM bright-field image showing Cu_2O precipitate and dislocation microstructure characterizing the etch pit arrays illustrated in Figure 11.

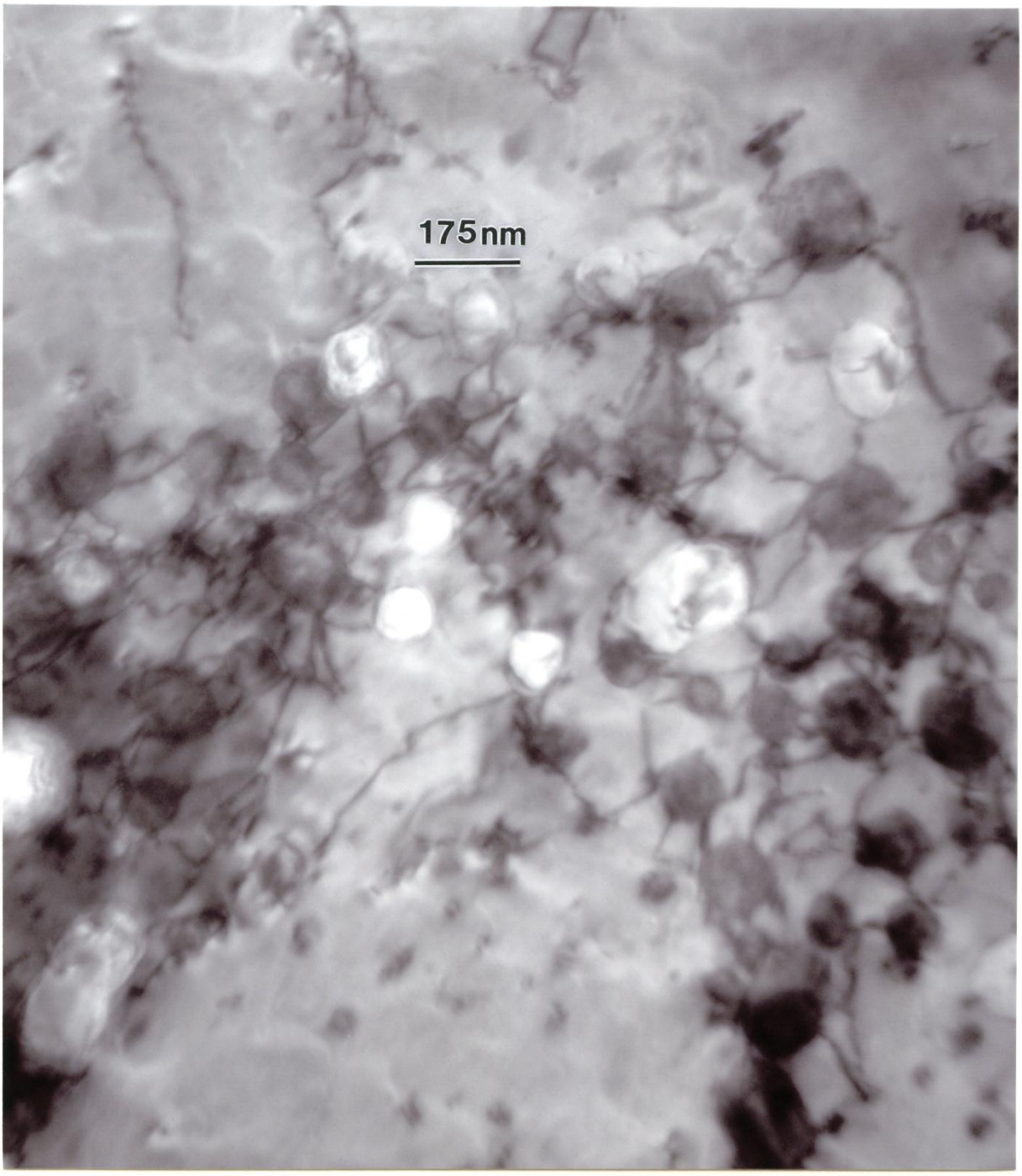

Figure 13. Magnified TEM image of cell-like microstructures in Figure 12. Note selective etching at Cu_2O precipitates as a precursor to forming etch-pit geometries in Figures 10 and 11.

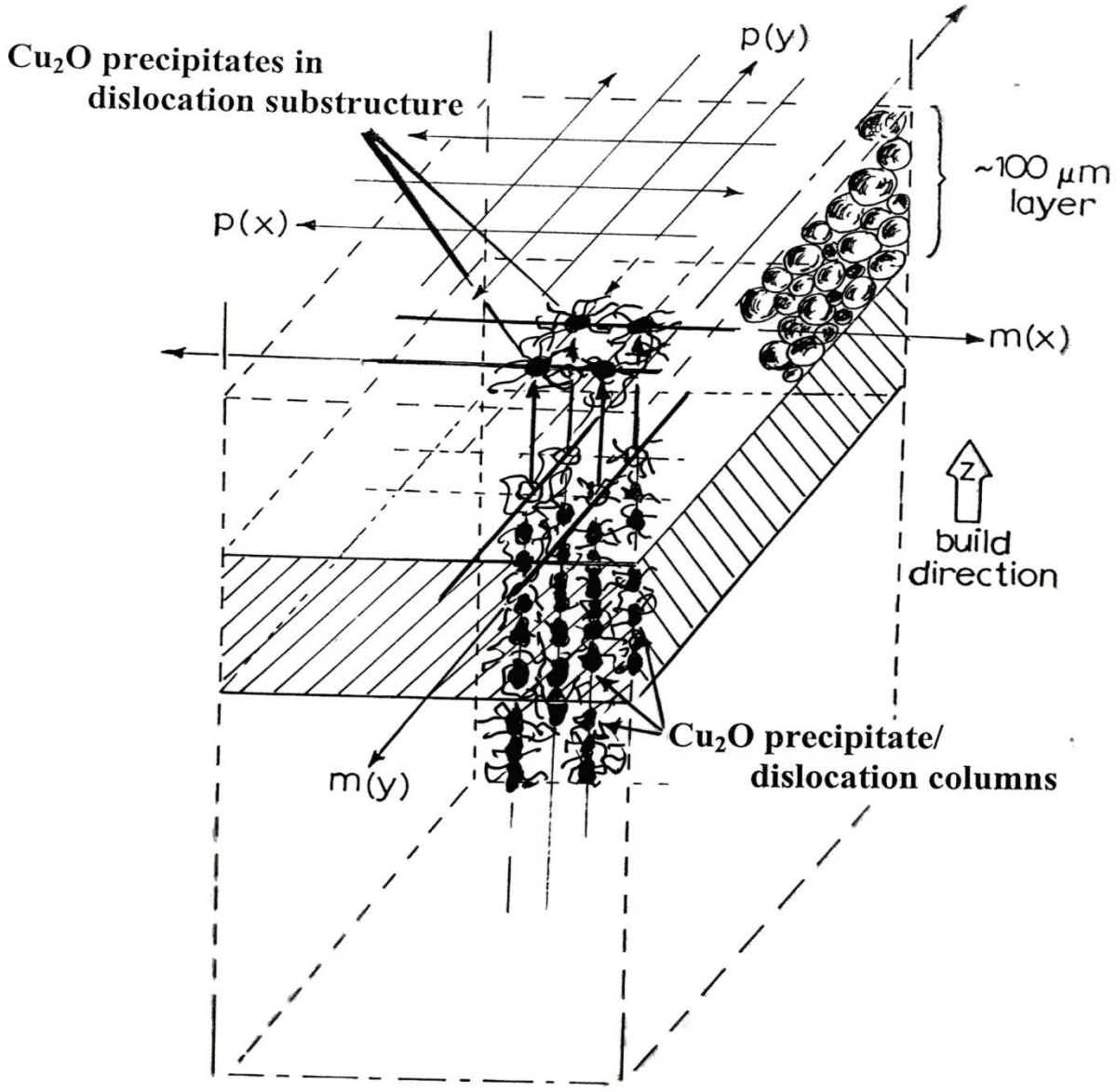

Figure 14. Schematic diagram depicting EBM electron beam scan geometry creating thermally requisite zones for creating or recognizing Cu_2O precipitates along with dislocation substructures forming architectures in build direction similar to Figure 4.

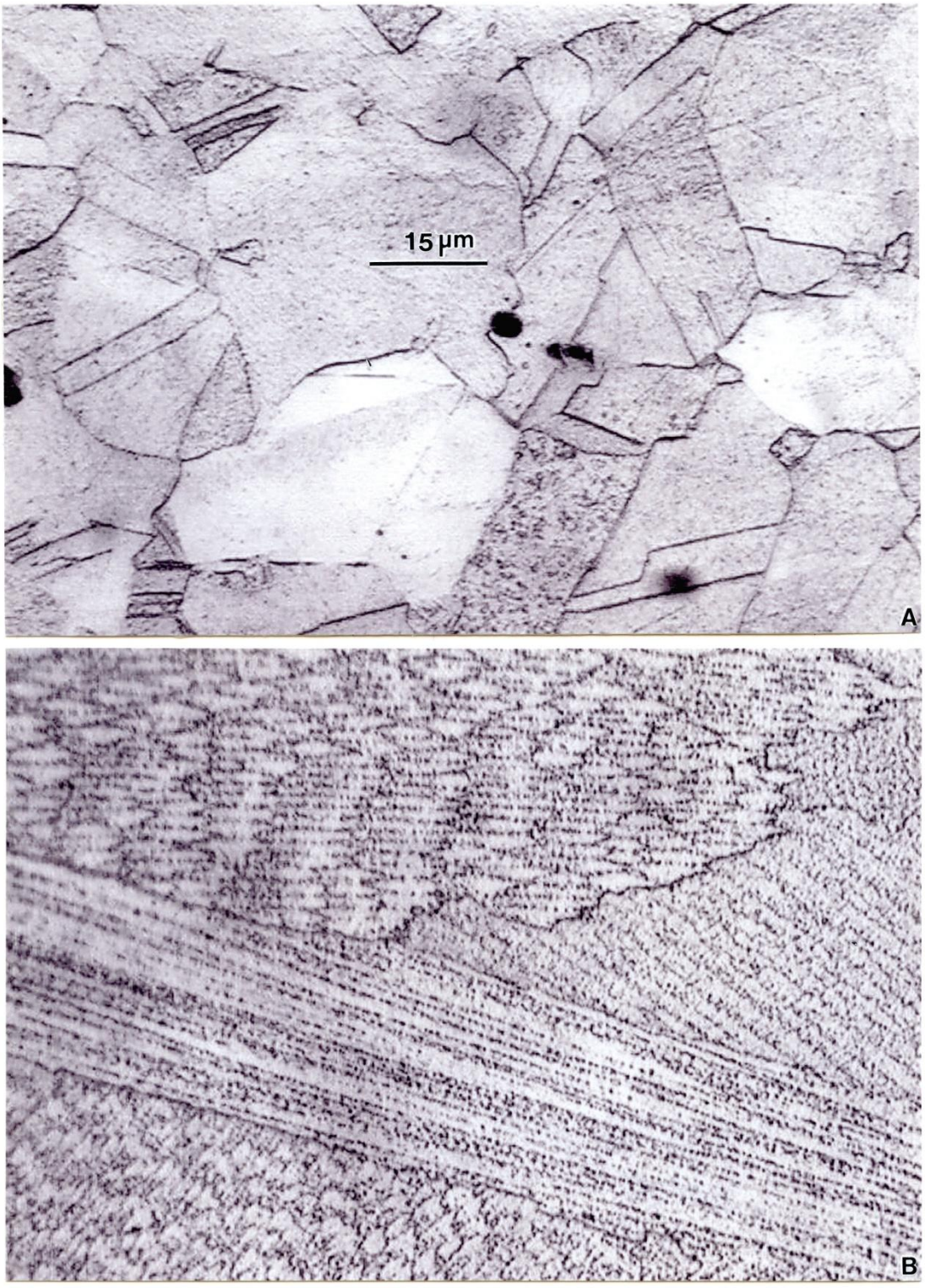

Figure 15. Optical metallograph image comparison for Cu base plate (A) showing equiaxed grain and coherent twin structures and EBM horizontal plane grain structures for fabricated Cu components.

Conceptual Al-Alloy Microstructural Architectures

A comparison of Figure 2 for the Co-base alloy and Figure 9 for the Cu containing Cu_2O precipitates illustrates some precipitate architecture similarities and differences. Comparison of Figures 4 and 14 suggest some process similarities associated with EBM fabrication where electron beam parameter variations (beam focus, current, scan rates, etc.) might systematically alter the spatial arrays and integrity of architectural columns or other structural geometries or systematic microstructure configurations or architectural predictions. Whether these features can be controlled for a range of systems is yet to be demonstrated. Figure 1D shows that, in comparison with other powders (Figures 1 B and C), other EBM process possibilities may exist. In the case of Al-6061 shown in its precursor powder form in Figure 1D, the wide range of microstructures which are developed in this alloy by thermomechanical treatment and aging may form similar microstructural architectures. Figure 16 illustrates examples of so-called Widmanstaaten microstructures created by aging in the range of 150 to 220°C by dense, thin precipitate plates coincident with specific crystal planes in the fcc crystal structure for bulk thermo-mechanically processed commercial Al-6061 alloy. In Figure 17A, prospects for more contiguous columnar precipitate architectures are illustrated for a higher carbon content in the Co-base alloy. Correspondingly, the selective precipitate formation in Al-6061 as suggested from Figure 16A and employing low-temperature EBM fabrication (as illustrated in Figures 4 and 14) might produce a columnar architecture as illustrated schematically in Figure 17B. Of course this is speculation based upon the observations for EBM component fabrication shown in Figures 2 to 6 for a Co-base alloy, and Figures 9 to 13 for oxygen-containing Cu. The suggestion for EBM fabrication for decreasing melting point powders implicit in Figure 1 B to D would follow: 1480°C, 1083°C and 647°C for the Co-base alloy, the Cu, and the Al-6061 respectively. Indeed, the low Al-6061 melting point and the low precipitation and aging temperatures may require a post-melt scan, although the friction-stir welding of Al-6061 where temperatures exceed $0.8T_M$ (T_M = melting temperature) exhibits a wide range of precipitation characteristics in the weld zone (Murr, 2010). The prospects for controlled microstructural architecture development by AM using EBM represents a revolutionary materials science and engineering concept extending the structure – properties – processing – performance paradigm.

Conclusions

These is strong evidence that AM using EBM may represent a processing route for controlled microstructural architecture in a number of metal and alloy systems. This revolutionary materials science and engineering concept could become an innovative extension of the structure – properties – processing – performance paradigm by the manipulation or optimization of EBM build parameters.

Acknowledgements

This research was supported in part by Mr. and Mrs. MacIntosh Murchison Endowments at The University of Texas at El Paso, and by AFRL contract No. UTEP 10-5567-013-02-C2 (Task Order 2.10.2) through Clarkson Aerospace, Inc. We thank Pedro Frigola of RadiaBeam Technologies for providing the copper powder.

References

Atamert, S. and Bhadeshia, H.K.D.H (1989). Comparison of the microstructure and abrasive wear properties of Stellite hardfacing alloys deposited by arc welding and laser cladding, Metallurgical and Materials Transactions, 20A: 1037-1054.

Crook, P. (1993). Cobalt, Cobalt Alloys, in ASM Metals Handbook, Vol. 2, Materials Park, Ohio, pp. 446-456.

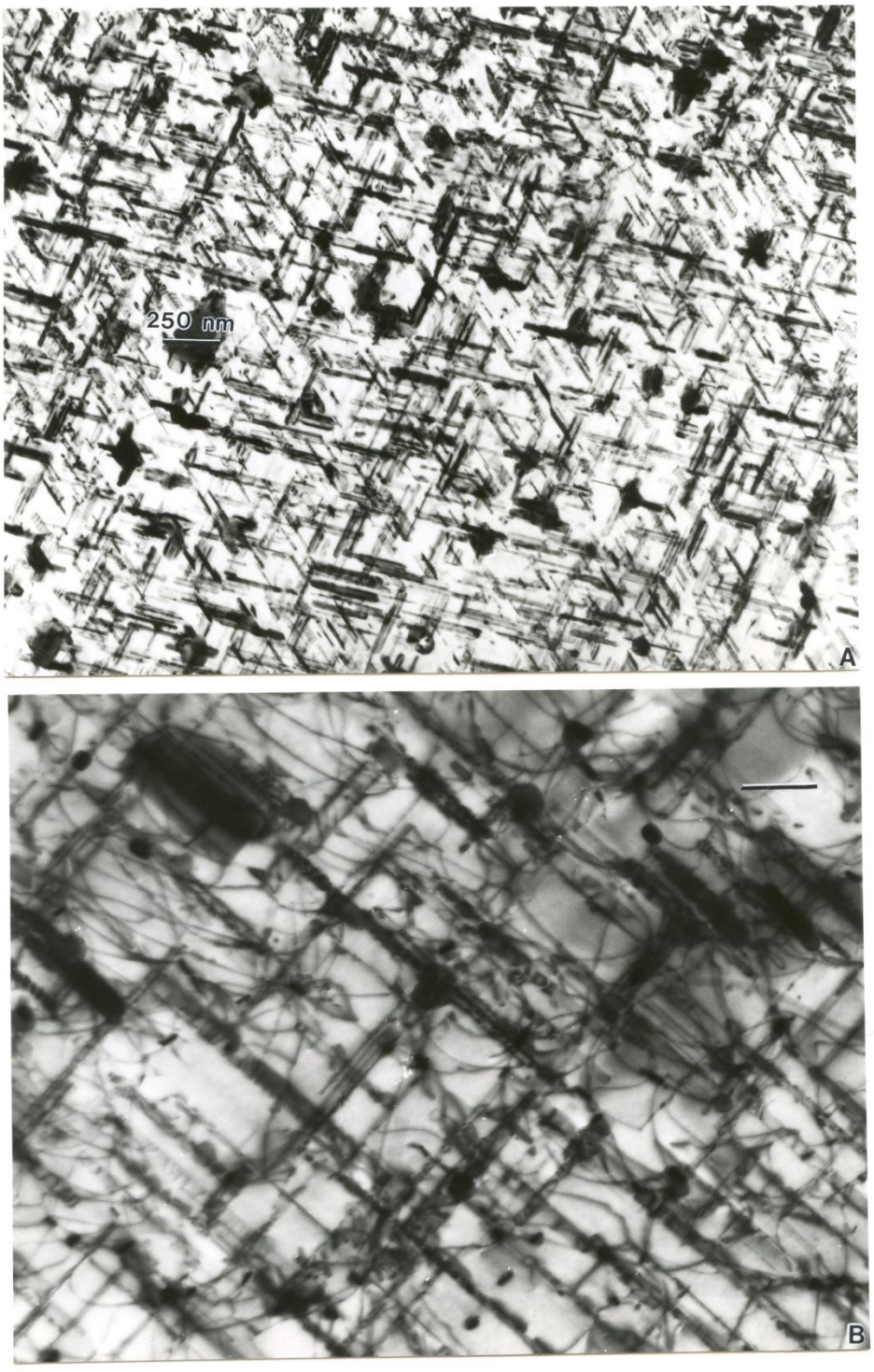

Figure 16. Examples of TEM bright-field images of coincident precipitate microstructures in Al-6061. (A) Dense, Widmanstaaten structures coincident with {111} planes. (B) precipitates coincident with {100} planes.

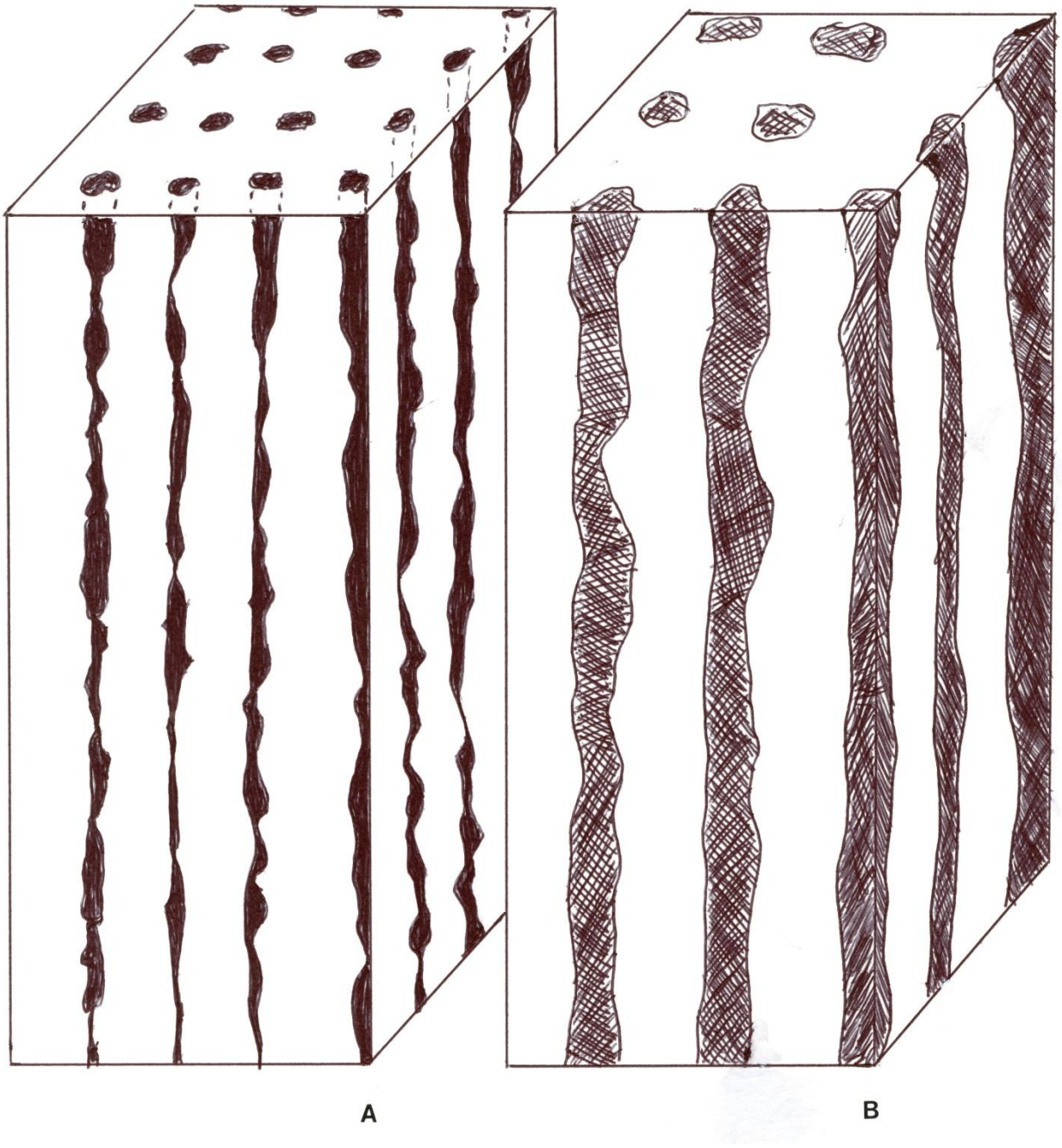

Figure 17. Schematic examples of columnar architectures created for dense precipitate arrays. (A) Dense carbide precipitates forming overlapping and continuous columnar microstructure for Co-base, high carbon content alloy. (B) Possible columnar arrays of Widmanstaaten precipitates in Al-6061 fabricated by EBM.

Gaytan, S. M., Murr, L. E., Martinez, E., Martinez, J. L., Machado, B. I., Ramirez, D. A., Medina, F., Collins, S., and Wicker, R. B., (2010a). Comparison of microstructures and mechanical properties for solid and mesh cobalt-base alloy prototypes fabricated by electron beam melting, Metallurgical and Materials Transactions A, in press.

Gaytan, S. M., Murr, L. E., Ramirez, D. A., Machado, B. I., Martinez, E., Hernandez, D. H., Martinez, J. L., Medina, F., and Wicker, R. B. (2010b). A TEM study of cobalt-base alloy prototypes with controlled microstructural architecture fabricated by EBM, to be published.

Murr, L. E., Esquivel E. V., Quinones, S. A., Gaytan, S. M., Lopez, M. I., Martinez, E. Y., Medina, F., Hernandez, D. H., Martinez, E., Martinez, J. L., Stafford, S. W., Brown, D. K., Hoppe, T., Meyers, W., Wicker, R. B., and Lindhe, U. (2009), Microstructure and mechanical properties of electron beam rapid-manufactured Ti-6Al-4V biomedical prototypes compared to wrought Ti-6Al-4V, Materials Characterization. 60: 96-105.

Murr, L. E., (2010). A review of FSW research on dissimilar metal and alloy systems. Journal of Materials Engineering and Performance, published online 02 February.

Ramirez, D. A., Murr, L. E., Martinez, E., Hernandez, D. A., Martinez, J. L., Machado, B. I., Medina, F., Wicker, R. B., Frigola, P., (2010).